Wave spectra of a strongly coupled magnetized one-component plasma: Quasilocalized charge approximation versus harmonic lattice theory and molecular dynamics

T. Ott,[1] D. A. Baiko,[2,3] H. Kählert,[4] and M. Bonitz[1]

[1]*Institut für Theoretische Physik und Astrophysik, Christian-Albrechts-Universität zu Kiel, Leibnizstraße 15, 24098 Kiel, Germany*

[2]*Ioffe Physical-Technical Institute, Politekhnicheskaya 26, 194021 St. Petersburg, Russia*

[3]*St. Petersburg State Polytechnical University, Politekhnicheskaya 29, 195251 St. Petersburg, Russia*

[4]*Department of Physics, Boston College, Chestnut Hill, Massachusetts 02467, USA*

(Received 17 December 2012; published 11 April 2013)

Two different approaches to the calculation of the wave spectra of magnetized strongly coupled liquid one-component plasmas are analzyed: the semianalytical quasilocalized charge approximation (QLCA) and the angle-averaged harmonic lattice (AAHL) theory. Both theories are benchmarked against the numerical evidence obtained from molecular dynamics simulations. It is found that not too far from the melting transition ($\Gamma \gtrsim 100$), the AAHL theory is superior to the QLCA, while further away from the transition, the QLCA performs comparably to or better than the AAHL theory.

DOI: 10.1103/PhysRevE.87.043102 PACS number(s): 52.27.Gr, 52.27.Lw

I. INTRODUCTION

Strongly coupled plasmas are an important class of plasmas that in recent years have been the focus of increasing research. In these plasmas the interparticle energy exceeds the thermal energy, which gives rise to a plethora of new physical effects. Examples of such plasmas in the laboratory are dusty plasmas [1], ions in traps [2], and ultracold neutral plasmas [3]. Examples from astrophysics include neutron star crusts, white dwarfs, and the interior of Jovian planets (see, e.g., Ref. [4]).

These plasmas are often subjected to an external magnetic field that significantly influences the dynamics of the charged particles as well as their collective behavior [5]. In the laboratory, external magnetic fields can be directly applied to the system. Furthermore, it was recently demonstrated that a rigid-body rotation of the plasma imposes an effective magnetization via the mathematical equivalence of the Lorentz and Coriolis forces [6,7].

Physical quantities that are affected by the complex interplay between a strong correlation and magnetization include thermodynamic and transport properties. For instance, the low-temperature specific heat of a magnetized one-component plasma crystal was shown to increase by orders of magnitude in strong magnetic fields [8]. As another example, the particle diffusion perpendicular to the field lines was shown to decay as $1/B$ for strong fields, whereas the field-parallel diffusion, which is unaffected in weakly coupled plasmas, decays algebraically with the decay exponent depending on the strength of the coupling [9]. This behavior is expected to be caused by collective excitations and similar effects are anticipated for other transport quantities. The study of the collective behavior of strongly magnetized plasmas close to but below the crystallization point is therefore of central importance for the understanding of such complex phenomena.

In this paper we wish to expand the theoretical model of the collective excitation spectra of strongly coupled plasmas in the magnetic field. The system under consideration is the one-component plasma (OCP), which is a paradigm for the behavior of plasmas [10,11]. For the magnetized OCP, several sum rules for the long-wavelength behavior of the dynamical structure factor have been derived previously [12–14]. Deep in the strongly coupled liquid phase, the collective modes of the OCP have been successfully described in the framework of the quasilocalized charge approximation (QLCA) [15,16]. Here we present a comparison between the QLCA and a complementary approach rooted in the harmonic lattice description of the magnetized OCP solids (Wigner crystal) [8]. Our goals are to test critically both the QLCA description and the harmonic lattice approach against numerical data and compare both approaches in terms of their general features and respective predictive powers.

The harmonic lattice approach allows for a purely analytical calculation of the wave spectra. However, the results obtained in this way are independent of the coupling strength and their applicability is limited by anharmonic effects in finite-temperature systems. In principle, the crystalline Wigner lattice is fundamentally different from the liquid phase. Consider the radial pair distribution function $g(r)$ [17] (Fig. 1). In the moderately coupled OCP, $\Gamma = 10$, the relative distribution of particles is practically uniform [$g(r) = 1$], except for the correlation hole at short distances. With increasing coupling ($\Gamma = 50$ and 150), gradually, a more structured particle configuration emerges, which is evidenced by departures of $g(r)$ from unity. The amplitude of these oscillations decays in the liquid regime. If the coupling is further increased, the OCP undergoes a phase transition to a solid. The pair distribution function of the lattice (plotted in Fig. 1 at $\Gamma = 180$ and labeled HL) is completely different. It shows pronounced oscillations corresponding to a well-defined sequence of shells of nearest neighbors, next-nearest neighbors, etc. The oscillations decay very slowly with r, indicating a long-range order.

To extend the established harmonic lattice theory of the magnetized OCP [8] to the liquid regime, we rely on the physical picture that a sufficiently strongly coupled liquid plasma is composed of randomly oriented microcrystalline patches [20,21]. A suitable averaging procedure over the relative orientations of the crystal axes, the magnetic field, and the wave vector should then result in an approximation of the liquid phase wave propagation [22].

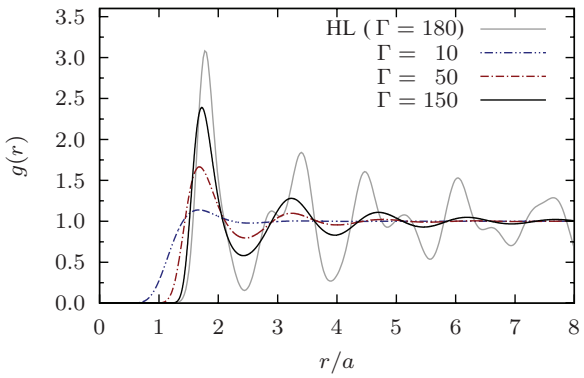

FIG. 1. (Color online) Pair distribution function $g(r)$ of the classical OCP from molecular dynamics simulation for $\Gamma = 10$, 50, and 150 and in the harmonic lattice approximation for the bcc lattice at $\Gamma = 180$ [18,19]. Distances are normalized to the Wigner-Seitz radius a (see Sec. II).

The remainder of this work is structured as follows. In Sec. II we introduce the model and its dimensionless parameters. In Sec. III we present the two theoretical methods of modeling the wave propagation in the OCP. We then introduce the numerical solution of the OCP by molecular dynamics simulation in Sec. IV. Both theories are benchmarked against the first-principles simulation results in Sec. V. We summarize in Sec. VI.

II. MAGNETIZED ONE-COMPONENT PLASMA MODEL

Our model is the classical one-component plasma with a neutralizing homogeneous background in which the particles are subjected to an external magnetic field $\mathbf{B} = B\mathbf{b}$ (B is the magnetic-field strength and $\mathbf{b}$ is the unit vector). The equations of motion read

$$\ddot{\mathbf{r}}_i = \mathbf{F}_i/m + \omega_c \mathbf{v}_i \times \mathbf{b}, \quad i = 1, \ldots, N, \tag{1}$$

where N is the number of particles, m their mass, $\omega_c = qB/m$ the cyclotron frequency, and q the particle charge. The equations are coupled via the Coulomb force $\mathbf{F}_i$ on particle i due to all other particles.

In thermodynamic equilibrium, the OCP is characterized by the single (coupling) parameter

$$\Gamma = \frac{q^2}{4\pi\varepsilon_0 a k_B T}, \tag{2}$$

where $a = (3/4n\pi)^{1/3}$ is the Wigner-Seitz radius with the number density n and T is the temperature. Generally, a OCP is considered strongly coupled whenever $\Gamma > 1$. It is known, however, that a substantial change in the characteristic dynamics occurs around $\Gamma_{\text{crit}} \approx 30$ [9,23], at which the so-called caging, i.e., negative portions in the velocity autocorrelation function or quasiclosed loops in phase space, occurs. It is this critical value that we consider as the boundary between a strongly coupled OCP and an intermediately coupled OCP (which are still considerably more highly correlated than weakly coupled systems $\Gamma < 1$).

A magnetized OCP is characterized by an additional parameter: the strength of the magnetic field. We take this as the ratio between the cyclotron and the plasma frequency $\beta = \omega_c/\omega_p$, where $\omega_p^2 = nq^2/\varepsilon_0 m$.

III. THEORETICAL APPROACHES

The dispersion relations for the eigenmodes of the magnetized OCP are given by solutions of a general equation of the type

$$\det\{\omega^2\delta_{\alpha\beta} - M_{\alpha\beta}(\mathbf{k}) - i\omega\omega_c\varepsilon_{\alpha\beta\gamma}b_\gamma\} = 0, \tag{3}$$

where $\omega(\mathbf{k})$ is the mode frequency, $\mathbf{b} = \mathbf{B}/B$, $\varepsilon_{\alpha\beta\gamma}$ is the Levi-Civita symbol, greek indices denote Cartesian components, and the matrix $M_{\alpha\beta}(\mathbf{k})$ depends on the chosen theoretical approach.

A. Harmonic lattice approximation

The harmonic lattice (HL) solution to the spectrum of the magnetized OCP has recently been analyzed in Ref. [8]. In the HL model, the OCP is assumed to form a perfect body-centered-cubic (bcc) lattice in space. The particles undertake small thermal excursions from their equilibrium positions. The matrix $M_{\alpha\beta}(\mathbf{k})$ of Eq. (3) is the dynamic matrix of the bcc lattice:

$$M_{\alpha\beta}(\mathbf{k}) = \frac{\omega_p^2}{3}\delta_{\alpha\beta} - \frac{q^2}{4\pi\varepsilon_0 m}\frac{\partial^2}{\partial u_\alpha \partial u_\beta}{\sum_{\mathbf{l}}}' \frac{e^{-i\mathbf{k}\cdot\mathbf{l}}}{|\mathbf{l}-\mathbf{u}|}, \tag{4}$$

where the derivative on the right-hand side is taken at $\mathbf{u} = 0$ (see, e.g., Refs. [18,24]). The summation is over all bcc lattice vectors $\mathbf{l}$, excluding $\mathbf{l} = 0$.

In the HL model, at each $\mathbf{k}$ there are three generally different solutions $\omega_{1,2,3}(\mathbf{k})$ of Eq. (3). They depend also on the strength and orientation of the magnetic field with respect to the crystal axes. To obtain a description of liquid systems (i.e., systems with rotational symmetry), we propose the angle-averaged harmonic lattice (AAHL) model. In this approach, the exact crystal dispersion curves obtained from the HL model undergo a two-step averaging procedure. First, we fix the magnetic-field direction with respect to the crystal axes and the angle Θ between $\mathbf{k}$ and $\mathbf{B}$. We then average $\omega(\mathbf{k})$ over the azimuthal angle of $\mathbf{k}$ with respect to $\mathbf{B}$. The three solutions (with minimum, intermediate, and maximum frequencies) are averaged separately. In the second step, we average over all nonequivalent directions of the magnetic field with respect to the crystal axes. This procedure is equivalent to analogous averaging for two-dimensional lattices [20,25,26]. Note that even though the averaging introduces an isotropy into the description, the theory is still based on the anisotropic ground state of the crystal.

The validity of applying a theory based on lattice configurations to the liquid state can be estimated by comparing the relevant time scales of the particle localization and the lifetime of the excited modes. The cage-decorrelation time t_c, i.e., the average time a particle spends in a crystal-like environment before undergoing larger excursions, has been measured in Ref. [27]. For $\Gamma > 100$, t_c exceeds $100\omega_p^{-1}$. This is much longer than the lifetime of any mode under

consideration (see, e.g., Figs. 4 and 5). Thus the particles experience a crystal-like environment during the entire lifetime of the mode. This argument in favor of the AAHL model is further strengthened by considering the relevant length scales. The typical cage size in a strongly coupled liquid exceeds the Wigner-Seitz radius a [27]. This means that modes with wavelengths below that (i.e., $ka \gtrsim 1$) propagate in a crystal-like environment.

Since the phonon frequencies in the harmonic bcc OCP crystal are strictly real, the angle-averaged frequencies are also real, which means an infinite lifetime of the respective excitations. This is not very realistic because anharmonic effects become stronger with a decrease of Γ and the associated phonon decay and merger processes would reduce the lifetime of the collective modes. In our approach we hope to describe correctly only the real parts of the excitation frequencies. Additionally, the dispersion curves obtained in this way are independent of Γ. This is also not very realistic for a strongly coupled liquid and thus the model may be expected to get worse with a decrease of Γ.

The phonon wave vector normally is limited to the first Brillouin zone, which corresponds roughly to $ka \approx 2.4$. If $\mathbf{k}$ goes beyond the first Brillouin zone, one can find the reciprocal lattice vector $\mathbf{G}$ such that $\mathbf{q} = \mathbf{k} - \mathbf{G}$ is in the first Brillouin zone. Then $\mathbf{q}$ is the actual phonon wave vector that determines its wavelength. For the sake of the dispersion curve approximation in the liquid at wavelengths shorter than what is allowed in the crystal (i.e., $ka \gtrsim 2.4$), we have to take $\mathbf{k}$ in our averaging procedure beyond the first Brillouin zone. This can easily result in situations where ions oscillating along $\mathbf{k}$ at the same time oscillate across $\mathbf{q}$. Besides that, generally, in a crystal, phonons have mixed polarizations oscillating neither along nor across their wave vector. Both effects introduce ambiguity into the frequency averaging procedure. Our procedure outlined above consists of sorting modes according to their frequencies. It is the simplest approach, but, as we shall see, it yields reasonable results. However, it may be worthwhile to investigate angular averaging taking into account phonon polarization in an effort to further improve the description of liquid dispersion curves within the AAHL model framework.

For illustration, a selection of crystal dispersion curves for various orientations of the wave vector with respect to the crystal axes for the OCP at zero magnetic field and for the OCP at $\beta = 1$ ($\mathbf{k} \parallel \mathbf{B}$) is shown in Fig. 2 (gray lines) together with the angle-averaged dispersion (black line). For each magnetization, there are two shear modes (left and middle columns) and one plasmon mode (right column). For $\beta = 0$, this is in contrast with the QLCA description of the system (see the next section), in which only a single degenerate shear mode is predicted.

B. Quasilocalized charge approximation

In the quasilocalized charge approximation (QLCA), the particle configuration considered is not necessarily periodic [16,21,28,29]. The momentary potential landscape is assumed to contain deep minima and to vary slowly on the time scales of the collective oscillations. The particles then experience a latticelike surrounding long enough to undergo a reasonable number of oscillations before lattice site diffusion takes place.

The generalization of the QLCA to magnetized three-dimensional OCPs has been presented in Ref. [15]. One has

$$M_{\alpha\beta}(\mathbf{k}) = \frac{k_\alpha k_\beta}{k^2}\omega_p^2 + D_{\alpha\beta}, \tag{5}$$

where the first term corresponds to the Vlasov part of the excitation while the correlational effects enter via the QLCA dynamical matrix

$$D_{\alpha\beta}(\mathbf{k}) = V^{-1}\sum_{\mathbf{q}} \frac{q_\alpha q_\beta}{|\mathbf{q}|^2}\omega_p^2[h(|\mathbf{k}-\mathbf{q}|) - h(|\mathbf{q}|)], \tag{6}$$

where V is the total volume and $h(k)$ is the Fourier transform of the pair correlation function $h(r) = g(r) - 1$. The pair correlation function provides information about the relative arrangement of the particles and is an external input to the QLCA, making the theory semianalytic. We use pair correlation functions obtained from first-principles molecular dynamics simulations to calculate the dispersion relations.

The analytic form of the solutions to Eq. (3) has been given in Ref. [15] for $\Theta = 0$ and $\pi/2$. These are the plasmon, the upper and lower shear modes ($\Theta = 0$), the ordinary shear mode, and the upper and lower hybrid modes ($\Theta = \pi/2$). Other (oblique) angles between $\mathbf{B}$ and $\mathbf{k}$ are not considered here, but are the subject of another work [30].

C. Direct thermal effects

Both the AAHL model and the QLCA do not include direct thermal effects, i.e., the Brownian motion of individual particles [the QLCA includes indirect thermal effects via the temperature dependence of $g(r)$]. The order of magnitude of the direct thermal effects is Γ^{-1}, so they can be safely neglected close to the melting transition. For lower values of Γ, they grow in importance and give rise, for example, to the Bohm-Gross term in the longitudinal dispersion.

To include these effects in the QLCA, we follow the prescription of Hou *et al.* [31] and replace ω_p^2 by $\omega_p^2 + 3k^2v_{\mathrm{th}}^2 = \omega_p^2[1 + (ka)^2/\Gamma]$ in the dispersion relation for the plasmon, where $v_{\mathrm{th}}^2 = kT/m$ is the square of the thermal velocity. This simple extension of the QLCA has shown remarkably good results in two-dimensional systems [31]. Here we test its suitability for a three-dimensional system.

IV. FIRST-PRINCIPLES SIMULATIONS

A. Molecular dynamics

Our simulation method is based on the exact simultaneous numerical solution of Eq. (1) for $N = 8196$ particles by molecular dynamics (MD) simulation. The advancement of individual particle trajectories takes places according to a generalized velocity Verlet scheme [32,33], which incorporates magnetic fields of arbitrary strength [9].

The particles are situated in a cubic simulation box with periodic boundary conditions and are brought into equilibrium during a thermostation phase in which the particles' velocities

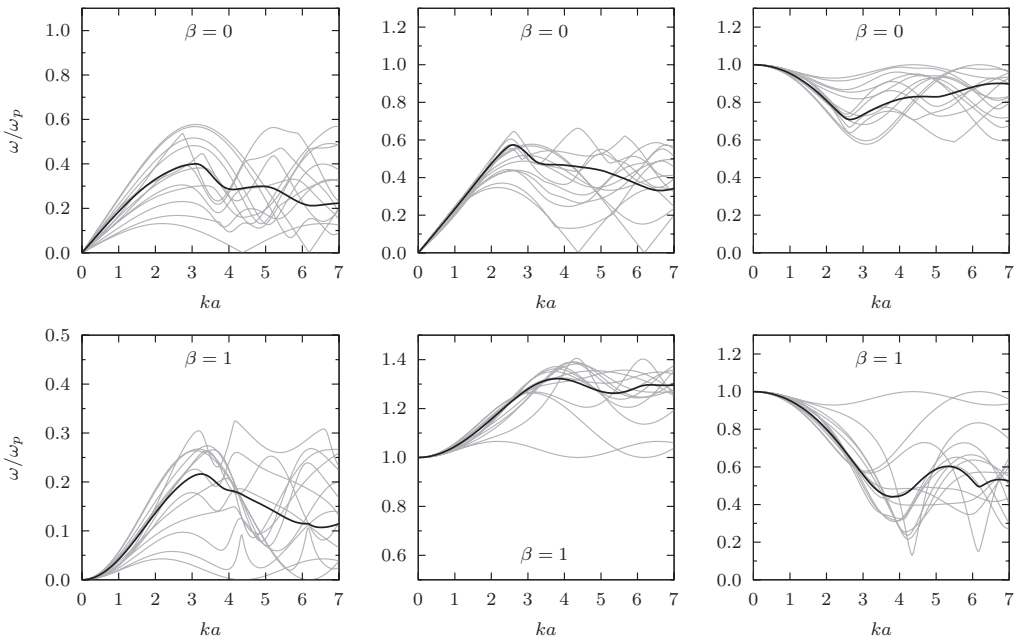

FIG. 2. Selection of the dispersion curves from the HL model for the unmagnetized (top row) and magnetized (bottom row, $\beta = 1$) OCP crystal for different directions of the wave vector with respect to the crystal geometry (gray lines). For the magnetized crystal, **k** is along **B**. The black lines show angle-averaged dispersion relations. The left and the middle column depict the (quasitransverse) shear modes and the rightmost column depicts the (quasilongitudinal) plasmon mode. Note that the mode shown in the bottom middle graph originates at $\omega = \omega_c = \omega_p$.

are rescaled continuously. During the data collection phase, the system evolves microcanonically. The interparticle forces are calculated according to the Ewald summation technique [34] to take into account correctly the long-range nature of the Coulomb potential. For each parameter set, we perform simulations spanning a time of $t\omega_p = 64\,000$.

B. Calculation of wave spectra

The parameters of the collective modes, i.e., long-lived thermally excited fluctuations, are obtained from the microscopic phase-space information of the system, specifically, from the Fourier analysis of the microscopic densities. For the current one has [35,36]

$$\mathbf{j}(k,t) = \sum_{j=1}^{N} \mathbf{v}_j(t) \exp[i\mathbf{k}\cdot\mathbf{r}_j(t)]. \tag{7}$$

One can also introduce longitudinal λ and transverse τ components of the current, e.g.,

$$\lambda(k,t) = \sum_{j=1}^{N} v_{xj}(t) \exp[ikx_j(t)], \tag{8}$$

$$\tau(k,t) = \sum_{j=1}^{N} v_{yj}(t) \exp[ikx_j(t)], \tag{9}$$

separating velocity components directed along and across the wave vector, respectively. [In Eqs. (8) and (9), **k** is assumed to be along the x axis.]

Introducing further the orientation of **j** with respect to the magnetic field **B**, we consider the five principal ($\Theta = 0$ and $\pi/2$) currents

$$\lambda^{\parallel}(k,t) = \sum_{j=1}^{N} v_{zj}(t) \exp[ikz_j(t)], \tag{10}$$

$$\tau_{\parallel}(k,t) = \sum_{j=1}^{N} v_{xj}(t) \exp[ikz_j(t)], \tag{11}$$

$$\lambda^{\perp}(k,t) = \sum_{j=1}^{N} v_{xj}(t) \exp[ikx_j(t)], \tag{12}$$

$$\tau_{\perp}^{\perp}(k,t) = \sum_{j=1}^{N} v_{yj}(t) \exp[ikx_j(t)], \tag{13}$$

$$\tau^{\parallel}(k,t) = \sum_{j=1}^{N} v_{zj}(t) \exp[ikx_j(t)], \tag{14}$$

where we have assumed, without loss of generality, $\mathbf{B} = B\hat{\mathbf{e}}_z$ and omitted the implicit replacements $\{x,y\} \to \{y,x\}$. The superscript in these quantities specifies the orientation of the particle velocity with respect to **B** and the subscript indicates the orientation of the wave vector with respect to **B** (see Fig. 3).

From these currents we obtain the fluctuation spectra in a standard manner via a temporal Fourier transform $\mathcal{F}_t$,

$$L = \frac{1}{2\pi N} \lim_{t\to\infty} \frac{1}{t} |\mathcal{F}_t\{\lambda(k,t)\}|^2, \tag{15}$$

$$T = \frac{1}{2\pi N} \lim_{t\to\infty} \frac{1}{t} |\mathcal{F}_t\{\tau(k,t)\}|^2, \tag{16}$$

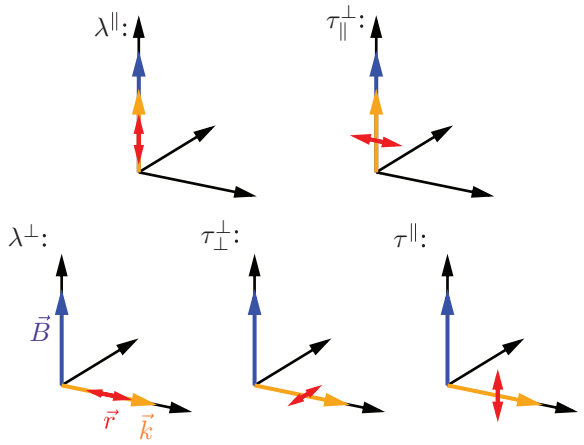

FIG. 3. (Color online) Relative orientation of the magnetic field [blue (dark) arrow], the wave vector [orange (light) arrow], and the particle velocity [red (two-headed) arrow] for the five currents (10)–(14).

which are furnished with the appropriate indices as above. Since our simulations extend over long-time periods, the frequency resolution is very high. We perform a suitable averaging to coarse grain these data and improve statistics. Permissible wave vectors are given by integer multiples of $|\mathbf{k}_{\min}| = 2\pi/L = 0.195/a$, as dictated by our use of periodic boundary conditions.

Collective excitations manifest themselves as peaks in the fluctuation spectra, where the peak width carries information about the longevity of the excitation. We extract the peak position and its full width at half maximum (FWHM) by fitting background-adjusted Gaussian functions to the simulation data.

V. RESULTS

A. Magnetized OCP

1. $\Gamma = 150$

We begin by considering the magnetized OCP close to the crystallization transition at $\Gamma = 150$ and $\beta = 1$ (Fig. 4). The five spectra (10)–(14) are calculated and $L^{\perp}(k,\omega)$ and $T_{\perp}^{\perp}(k,\omega)$ are summed to capture the mixed polarization of the upper and lower hybrid modes [15,31].

In Fig. 4, the resulting four fluctuation spectra are shown as density plots (blue), together with the numerical peak positions (symbols) and theoretical predictions from the QLCA [black (dark) solid lines] and the AAHL model [red (light) solid lines]. The FWHM of the numerical peaks is indicated by the horizontal black bars. Narrow peaks (small FWHM) correspond to long-lived excitations and broad peaks (large FWHM) indicate short-lived waves.

In the $L^{\perp} + T_{\perp}^{\perp}$ spectrum (top graph) the upper hybrid mode (higher frequency) and the lower hybrid mode (lower frequency) stand out clearly in the numerical data. The upper hybrid mode originates at $\omega = (\omega_p^2 + \omega_c^2)^{1/2}$ at $ka = 0$ [15] with a very narrow peak structure indicating long-lived oscillations. The frequency of the oscillations slightly decreases for shorter wavelengths and the damping increases (larger width of the peaks).

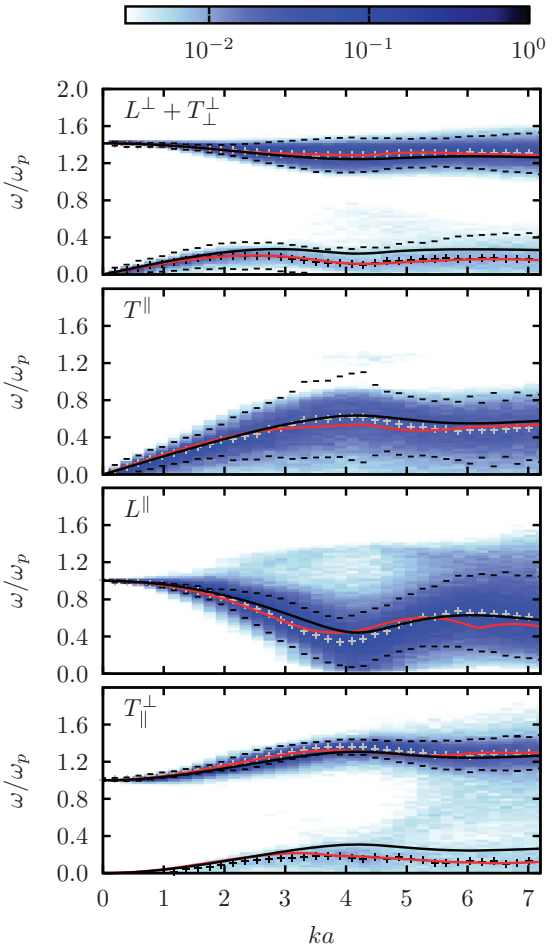

FIG. 4. (Color online) Collective excitation spectra of the magnetized OCP at $\Gamma = 150$ and $\beta = 1$. The color scale corresponds to simulation results, the black and gray symbols mark the simulation peak maxima, and the black bars are their FWHM. The solid lines indicate the QLCA [black (dark)] and AAHL model [red (light)] dispersion relations.

Both the QLCA and the AAHL model agree up to $ka \approx 3$ and correctly predict the course of the upper hybrid mode. For higher values of ka, the QLCA deviates from the numerical data and underestimates the involved frequencies. The AAHL approach, in contrast, is in excellent agreement with the simulations, a remarkable result showing the applicability of our angle-averaging procedure.

The low-frequency lower shear mode is similarly perfectly predicted by the AAHL model, even though the oscillations of the lower shear mode are strongly damped and short lived. The QLCA dispersion relation is in agreement with the numerical data for long wavelengths, but overestimates the frequencies of the lower shear mode for $ka \gtrsim 2$. Such a decreased reliability of the QLCA for low-frequency modes has been often noted [15,21] and was commonly attributed to the diffusion and dissolution of the potential cages, which are fundamental to the theory, on these long-time scales. However, as the AAHL model does not include any of these effects either, it seems plausible that another inherent property of the QLCA limits its applicability in the low-frequency regime.

The ordinary shear mode (second graph of Fig. 4) originates at zero frequency and rises to a maximum around $ka = 4$ with $\omega \approx 0.6\omega_p$. The QLCA correctly predicts the position and height of this maximum and is in good agreement with the positions of the broad numerical peaks. The AAHL model prediction is equivalently good up to about $ka = 3$, after which the amplitude of the maximum is underestimated.

In the third graph, the plasmon mode originating at ω_p exhibits the typical correlation-induced negative slope leading to the so-called roton minimum and subsequent oscillations [21,37,38]. Both the QLCA and AAHL model predictions are in good agreement with the simulated spectrum.

The upper and lower shear modes (bottom graph) originate at $\omega = \omega_c = \omega_p$ and $\omega = 0$, respectively. It is again striking how well the AAHL model describes both of these modes, with a very close tracking of the numerical mode dispersion. Deviations occur for the low-frequency mode for $ka \lesssim 3$. The QLCA description is similarly good for the upper shear mode, but is again less reliable at low frequencies.

Overall, the predictive power of the QLCA and especially that of the AAHL model is very good and for the AAHL model it is much better than one might have expected. We hypothesize that the reason for this lies in the reduced mobility of the individual particles due to the magnetic field. It was recently demonstrated that in strongly coupled plasmas the diffusion both parallel and perpendicular to the magnetic field is greatly reduced (as opposed to weakly coupled plasmas, in which only the cross-field diffusion is affected by the magnetic field, as noted in the Introduction) [9]. For $\Gamma = 100$, the field-parallel diffusion coefficient is less than 40% and the cross-field diffusion coefficient is less than 30% of the field-free diffusion coefficient [9]. This reduced particle migration increases the predictive powers of theories based on lattice or latticelike structures.

2. $\Gamma = 50$ *and* 100

The applicability of the AAHL model and the QLCA to less strongly coupled OCPs is investigated in Figs. 5 and 6 for $\Gamma = 100$ and 50 at $\beta = 1$. It is evident that even at these values of the coupling parameter, the AAHL model and

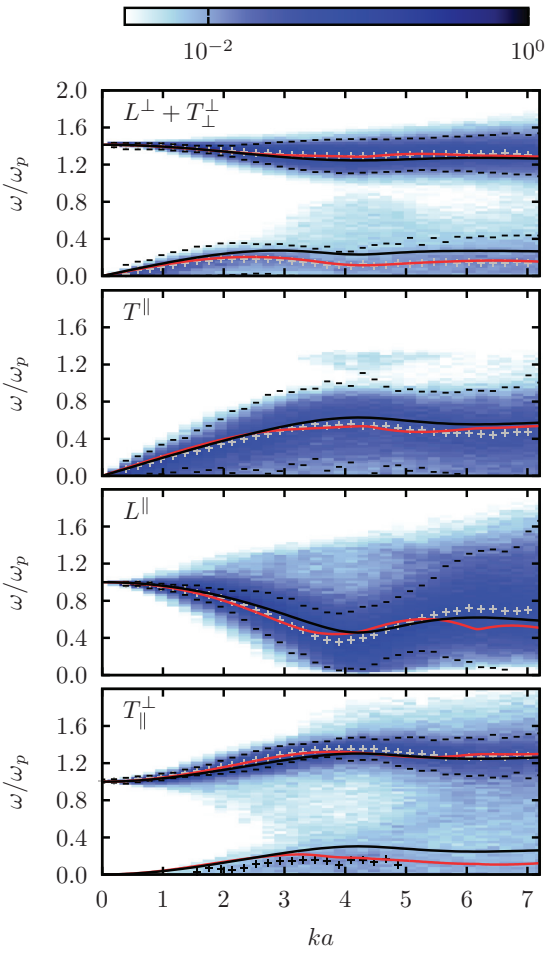

FIG. 5. (Color online) Collective excitation spectra of the magnetized OCP at $\Gamma = 100$ and $\beta = 1$. The color scale corresponds to simulation results, the black and gray symbols mark the simulation peak maxima, and the black bars are their FWHM. The solid lines indicate the QLCA [black (dark)] and AAHL model [red (light)] dispersion relations.

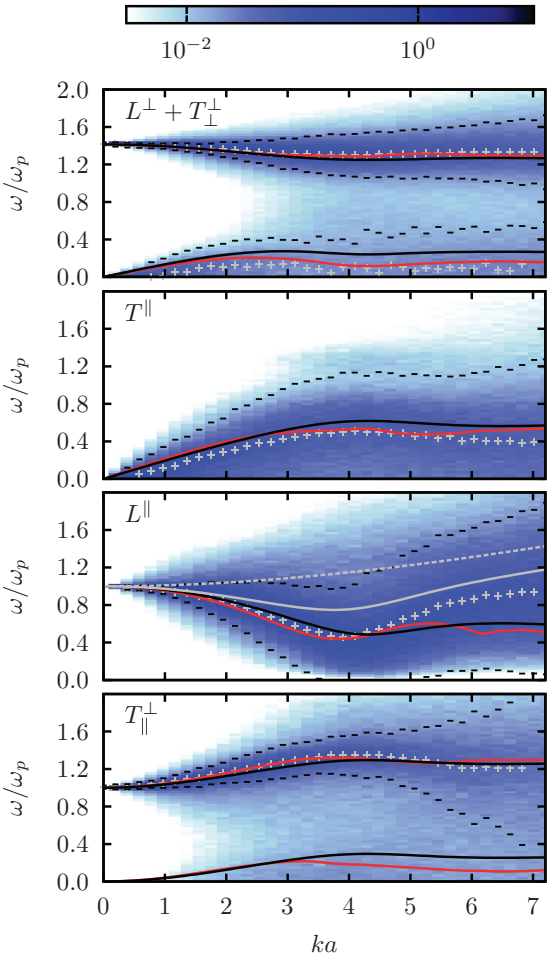

FIG. 6. (Color online) Collective excitation spectra of the magnetized OCP at $\Gamma = 50$ and $\beta = 1$. The color scale corresponds to simulation results, the symbols mark the simulation peak maxima, and the black bars are their FWHM. The solid lines indicate the QLCA [black (dark)] and AAHL model [red (light)] dispersion relations. The gray lines in $L^{\parallel}$ show the Bohm-Gross dispersion (dashed) and Bohm-Gross corrected QLCA results (solid) (Sec. III C).

the QLCA provide excellent descriptions of the dispersion relations. However, the gradual vanishing of the lower shear mode [low-frequency mode in $T_{\parallel}^{\perp}(k,\omega)$] as Γ decreases is not captured by the theories.

A notable exception of the predictive power of the theories presents itself in the $L^{\parallel}$ spectrum for $\Gamma = 50$, in which the numerical peak position is at much higher frequencies for large ka. This is a manifestation of direct thermal effects that become relevant at small coupling values. According to the approach of Sec. III C, direct thermal effects can be accounted for approximately in the QLCA by including a Bohm-Gross term in the dispersion relation. The gray lines in Fig. 6 indicate the course of the Bohm-Gross term (dashed line) and the extended QLCA approach (solid line). It is apparent that the trend of the dispersion relation change is correct, but the actual agreement with the numerical data is unsatisfactory, in contrast to what has been reported for two-dimensional systems [31].

We now consider the effect of a variation of the magnetic-field strength. Figure 7 depicts the system at $\Gamma = 150$ and

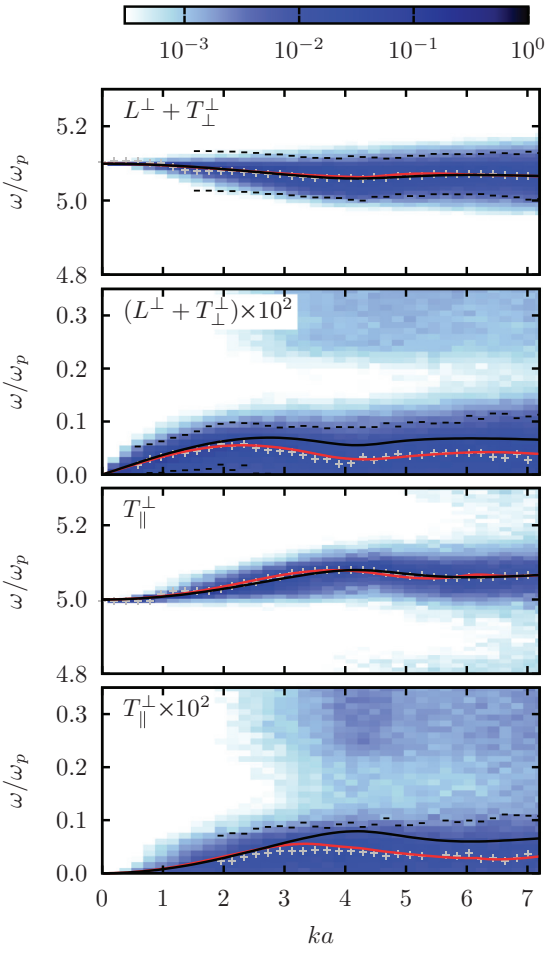

FIG. 7. (Color online) Collective excitation spectra of the magnetized OCP at $\Gamma = 150$ and $\beta = 5$. The color scale corresponds to simulation results, the symbols mark the simulation peak maxima, and the black bars are their FWHM. The solid lines indicate the QLCA [black (dark)] and AAHL model [red (light)] dispersion relations. Note the different ranges of the frequency axes and the 100-fold magnification of two of the spectra.

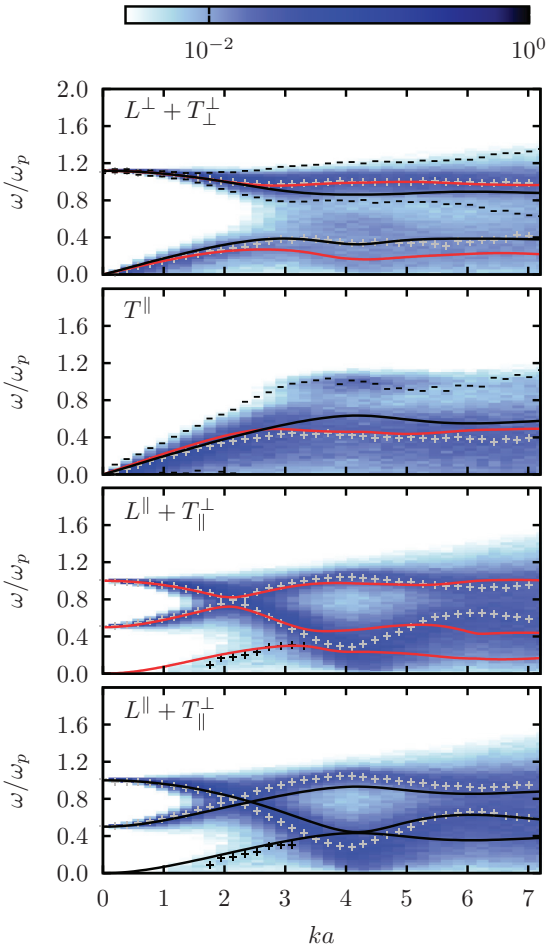

FIG. 8. (Color online) Collective excitation spectra of the magnetized OCP at $\Gamma = 150$ and $\beta = 0.5$. The color scale corresponds to simulation results, the black and gray symbols mark the simulation peak maxima, and the black bars are their FWHM. The solid lines indicate the QLCA [black (dark)] and AAHL model [red (light)] dispersion relations.

$\beta = 5$. Only two of the four previously considered spectra are shown, but at two different frequency ranges (the two omitted spectra show little difference from Fig. 4). For the high-frequency modes, the QLCA and the AAHL model agree practically perfectly with one another and with the numerical data. The weakly excited low-frequency branches (note the 100-fold magnification) are well described by the AAHL model.

At $\beta = 0.5$ (Fig. 8) the modes are less separated (we plot the sum of $L^{\parallel}$ and $T_{\parallel}^{\perp}$ to account for this fact). The quantitative agreement between the theoretical approaches and the numerical data is comparable to the case of $\beta = 1$, which suggests that the AAHL model is a feasible approach in the low-magnetic-field regime as well. To corroborate this, we consider the unmagnetized OCP next.

B. Unmagnetized OCP

Although much research has focused on the theoretical description of the unmagnetized OCP dispersion relations, reliable numerical data are still sparse (see, e.g., Refs. [21,39]).

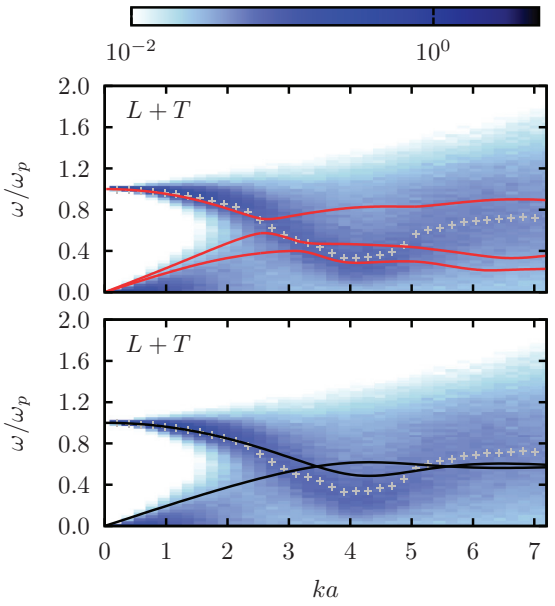

FIG. 9. (Color online) Collective excitation spectra of the unmagnetized OCP at $\Gamma = 50$. The color scale corresponds to simulation results and the symbols mark the simulation peak maxima (both figures contain the same MD data). The solid lines indicate the AAHL model (top) and QLCA (bottom) dispersion relations.

In Figs. 9 and 10 we show the numerical fluctuation spectra and peak positions together with the theoretical predictions of the QLCA and the AAHL model.

Consider first the case of $\Gamma = 50$ (Fig. 9). The transverse (acoustic) mode is not developed at this coupling, whereas the longitudinal plasmon is clearly observable and exhibits

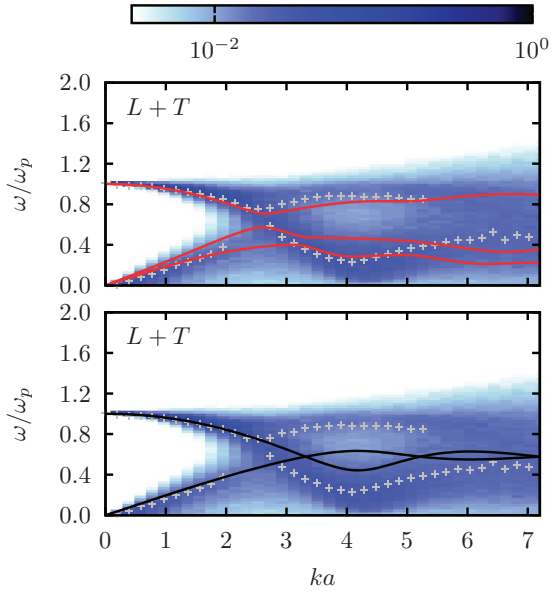

FIG. 10. (Color online) Collective excitation spectra of the unmagnetized OCP at $\Gamma = 150$. The color scale corresponds to simulation results and the symbols mark the simulation peak maxima (both figures contain the same MD data). The solid lines indicate the AAHL model (top) and QLCA (bottom) dispersion relations.

the typical correlational modifications. The AAHL model (top graph) turns out to be in quantitative agreement at small wave vectors, but is not applicable beyond $ka \approx 2$. Note that in many situations of practical interest, these wavelengths actually play the most important role. The QLCA description (bottom graph) is more appropriate and is in qualitative agreement for almost the entire range of the wavelengths, but the roton minimum and the subsequent rise are underestimated [38].

At higher coupling and close to the crystallization $\Gamma = 150$ (Fig. 10), the transverse mode is fully developed and correctly described by both the AAHL model and the QLCA at long wavelengths $ka \lesssim 2.5$. Since the liquid cannot sustain shear in the limit of $k \to 0$, the transverse mode vanishes for very long wavelengths in the numerical data but remains finite in the QLCA and the AAHL model. At shorter wavelengths, the AAHL model compares favorably to the numerical data for $ka \lesssim 5$, although only two (not three) distinct modes can be observed in the liquid phase. The QLCA is only in qualitative agreement at $ka \gtrsim 2.5$, overestimating the lower frequencies and underestimating the higher frequencies.

VI. CONCLUSION

It has been long known that correlations between individual particles in dense or cold plasmas give rise to fascinating phenomena such as the emergence of new collective oscillation modes. Strong magnetic fields often permeate plasmas and significantly alter their dynamic properties. With this work we have provided an extensive overview of the oscillation spectra in plasmas in which both of these conditions, i.e., strong coupling and magnetization, coexist. We have focused on the particularly interesting liquid regime, in which neither perturbational nor lattice calculations are pertinent.

Two theoretical descriptions—the quasilocalized charge approximation and the angle-averaged harmonic lattice theory—have been tested against extensive molecular dynamics simulations of the one-component plasma. While the QLCA is able to describe liquid structures in a semianalytic calculation (external information about the structure is used in the form of the pair distribution function), the AAHL model rests on a purely analytical footing and does not account for decay of correlations as Γ is lowered.

Nonetheless, we have found that in the magnetized OCP, the AAHL model provides an excellent description of the actual dispersion relations and can achieve similar or in some cases better agreement with the simulation data than the QLCA. This is likely due to the increased rigidity of magnetized systems, which makes a lattice calculation more appropriate. It is noted that this is an effect of the combined influence of strong correlations and strong magnetic fields: The particle coupling serves to isotropize the localizing effects of the magnetic field, as indicated by the decay of the diffusivity along the field lines [9].

We have also briefly tested the applicability of the QLCA and the AAHL model to unmagnetized systems at different couplings and have found that the range of validity of the QLCA is larger than that of the AAHL model and extends to considerably lower values of the coupling strength. Close to the freezing transitions, the AAHL model becomes

competitive again and provides a good description of the wave dispersions.

Finally, we have considered the influence of the direct thermal effects at smaller values of the coupling strength. The modification of the QLCA dispersion relation with the Bohm-Gross term [40] is a simple remedy for the increasing discrepancy between the QLCA and the simulation results that, however, fares somewhat worse in the three-dimensional OCP than it has in the two-dimensional case [40]. Other work will aim to provide a clearer description of these effects [39].

ACKNOWLEDGMENTS

This work was supported by the DFG via SFB-TR 24 (Projects No. A5 and No. A7) and Grant No. shp00006 for CPU time at the North-German Supercomputing Alliance HLRN. H.K. acknowledges support from the DAAD via a postdoctoral fellowship. The work of D.A.B. was supported by the Ministry of Education and Science of the Russian Federation (Contract No. 11.G34.31.0001, Agreement No. 8409), by RFBR (Grant No. 11-02-00253-a), and by Rosnauka (Grant No. NSh 4035.2012.2).

[1] M. Bonitz, C. Henning, and D. Block, Rep. Prog. Phys. **73**, 066501 (2010).
[2] M. J. Jensen, T. Hasegawa, J. J. Bollinger, and D. H. E. Dubin, Phys. Rev. Lett. **94**, 025001 (2005).
[3] T. Killian, T. Pattard, T. Pohl, and J. Rost, Phys. Rep. **449**, 77 (2007).
[4] S. L. Shapiro and S. A. Teukolsky, *Black Holes, White Dwarfs and Neutron Stars: The Physics of Compact Objects* (Wiley-Interscience, New-York, 1983).
[5] By virtue of the Bohr–van Leuween theorem, static properties of classical systems do not depend on the magnetic field.
[6] H. Kählert, J. Carstensen, M. Bonitz, H. Löwen, F. Greiner, and A. Piel, Phys. Rev. Lett. **109**, 155003 (2012).
[7] M. Bonitz, H. Kählert, T. Ott, and H. Löwen, Plasma Sources Sci. Technol. **22**, 015007 (2013).
[8] D. A. Baiko, Phys. Rev. E **80**, 046405 (2009).
[9] T. Ott and M. Bonitz, Phys. Rev. Lett. **107**, 135003 (2011).
[10] S. Ichimaru, Rev. Mod. Phys. **54**, 1017 (1982).
[11] S. Ichimaru, H. Iyetomi, and S. Tanaka, Phys. Rep. **149**, 91 (1987).
[12] L. Suttorp and A. Schoolderman, Physica A **141**, 1 (1987).
[13] B. Jancovici, N. Macris, and P. Martin, J. Stat. Phys. **47**, 229 (1987); P. A. Martin, Rev. Mod. Phys. **60**, 1075 (1988).
[14] R. Genga, Int. J. Theor. Phys. **27**, 819 (1988).
[15] T. Ott, H. Kählert, A. Reynolds, and M. Bonitz, Phys. Rev. Lett. **108**, 255002 (2012); see also G. Kalman, K. I. Golden, and M. Minella, in *Strongly Coupled Plasma Physics*, edited by H. M. Van Horn and S. Ichimaru (University of Rochester Press, Rochester, 1994).
[16] G. Kalman and K. I. Golden, Phys. Rev. A **41**, 5516 (1990).
[17] J. Hansen and I. McDonald, *Theory of Simple Liquids* (Academic, London, 2006).
[18] D. A. Baiko, D. G. Yakovlev, H. E. DeWitt, and W. L. Slattery, Phys. Rev. E **61**, 1912 (2000).
[19] A. I. Chugunov, D. A. Baiko, D. G. Yakovlev, H. E. DeWitt, and W. L. Slattery, Physica A **323**, 413 (2003).
[20] T. Sullivan, G. J. Kalman, S. Kyrkos, P. Bakshi, M. Rosenberg, and Z. Donkó, J. Phys. A: Math. Gen. **39**, 4607 (2006).
[21] Z. Donkó, G. J. Kalman, and P. Hartmann, J. Phys.: Condens. Matter **20**, 413101 (2008).
[22] An analogous procedure for the unmagnetized two-dimensional OCP with a Yukawa interaction was carried out in Ref. [20].
[23] J. Daligault, Phys. Rev. Lett. **96**, 065003 (2006).
[24] D. A. Baiko, A. Y. Potekhin, and D. G. Yakovlev, Phys. Rev. E **64**, 057402 (2001).
[25] P. Hartmann, Z. Donkó, G. Kalman, S. Kyrkos, M. Rosenberg, and P. Bakshi, IEEE Trans. Plasma. Sci. **35**, 337 (2007).
[26] G. J. Kalman, P. Hartmann, Z. Donkó, and K. I. Golden, Phys. Rev. Lett. **98**, 236801 (2007).
[27] Z. Donkó, P. Hartmann, and G. J. Kalman, Phys. Plasmas **10**, 1563 (2003).
[28] K. I. Golden and G. J. Kalman, Phys. Plasmas **7**, 14 (2000).
[29] G. J. Kalman, K. I. Golden, Z. Donkó, and P. Hartmann, J. Phys.: Conf. Ser. **11**, 254 (2005).
[30] H. Kählert, T. Ott, A. Reynolds, G. J. Kalman, and M. Bonitz, Phys. Plasmas (in press).
[31] L.-J. Hou, P. K. Shukla, A. Piel, and Z. L. Mišković, Phys. Plasmas **16**, 073704 (2009).
[32] S. A. Chin, Phys. Rev. E **77**, 066401 (2008).
[33] Q. Spreiter and M. Walter, J. Comput. Phys. **152**, 102 (1999).
[34] M. Deserno and C. Holm, J. Chem. Phys. **109**, 7678 (1998).
[35] J. P. Hansen, I. R. McDonald, and E. L. Pollock, Phys. Rev. A **11**, 1025 (1975).
[36] J. Boon and S. Yip, *Molecular Hydrodynamics* (Courier Dover, New York, 1991).
[37] K. I. Golden, G. Kalman, and P. Wyns, Phys. Rev. A **46**, 3454 (1992).
[38] G. J. Kalman, P. Hartmann, K. I. Golden, A. Filinov, and Z. Donkó, Europhys. Lett. **90**, 55002 (2010).
[39] J. P. Mithen, J. Daligault, and G. Gregori, Phys. Rev. E **85**, 056407 (2012).
[40] L.-J. Hou, Z. L. Mišković, A. Piel, and M. S. Murillo, Phys. Rev. E **79**, 046412 (2009).